Optical Imaging of Visual Cortical Responses Evoked by Transcorneal Electrical Stimulation With Different Parameters

Zengguang Ma,[1] Pengjia Cao,[1] Pengcheng Sun,[1] Liming Li,[1] Yiliang Lu,[2] Yan Yan,[1] Yao Chen,[1] and Xinyu Chai[1]

[1]School of Biomedical Engineering, Shanghai Jiao Tong University, Shanghai, China
[2]Institute of Neuroscience and State Key Laboratory of Neuroscience, Shanghai Institutes for Biological Sciences, Chinese Academy of Sciences, Shanghai, China

Correspondence: Xinyu Chai, Wenxuan Medical Building, RM 503 800 Dongchuan Road, Shanghai, 200240, China;
xychai@sjtu.edu.cn.
Yao Chen, Wenxuan Medical Building, RM 503 800 Dongchuan Road, Shanghai, 200240, China;
yao.chen@sjtu.edu.cn.

ZM and PC contributed equally to the work presented here and should therefore be regarded as equivalent authors.

Submitted: April 15, 2014
Accepted: July 17, 2014

Citation: Ma Z, Cao P, Sun P, et al. Optical imaging of visual cortical responses evoked by transcorneal electrical stimulation with different parameters. *Invest Ophthalmol Vis Sci*. 2014;55:5320–5331. DOI: 10.1167/iovs.14-14600

Purpose. The use of phosphenes evoked by transcorneal electrical stimulation (TcES) has been proposed as a means of residual visual function evaluation and candidate selection before implantation of retinal prostheses. Compared to the subjective measures, measurement of neuronal activity in visual cortex can objectively and quantitatively explore their response properties to electrical stimulation. The purpose of this study was to investigate systematically the properties of cortical responses evoked by TcES.

Methods. The visual cortical responses were recorded using a multiwavelength optical imaging of intrinsic signals (OIS) combining with electrophysiological recording by a multichannel electrode array. The effects of different parameters of TcES on cortical responses, including the changes of hemoglobin oxygenation and cerebral blood volume, were examined.

Results. We found consistent OIS activation regions in visual cortex after TcES, which also showed strong evoked field potentials according to electrophysiological results. The OIS response regions were located mainly in cortical areas representing peripheral visual field. The extent of activation areas and strength of intrinsic signals were increased with higher current intensities and longer pulse widths, and the largest responses were acquired in the frequency range 10 to 20 Hz.

Conclusions. Use of TcES through the ERG-jet corneal electrode may preferentially activate peripheral retina. Revealing the hemodynamic changes in visual cortex occurred after electrical stimulation can contribute to comprehension of neurophysiological underpinnings underlying prosthetic vision. This study provided an objective foundation for optimizing parameters of TcES and would bring considerable benefits in the application of TcES for assessment and screening in patients.

Keywords: multiwavelength optical imaging, transcorneal electrical stimulation, visual cortical responses

Visual prostheses aim to elicit phosphenes by electrically stimulating different locations along the visual pathway and offer a potential therapeutic option for restoring functional vision for patients suffering from retinal degeneration.[1] At present, retinal prostheses have been demonstrated to be most promising approaches and the Argus II epiretinal prosthesis had been approved by European CE and the United States Food and Drug Administration for treating severe retinitis pigmentosa (RP) patients.[2] As retinal prostheses have been applied in clinical practice, the need for preimplantation selection is becoming increasingly important to define an effective rehabilitative strategy and promote rehabilitative success.[3]

Potts et al.[4] have demonstrated that transcorneal electrical stimulation (TcES) can evoke phosphenes and electrically evoked responses from the occipital lobe. Some studies have indicated that TcES mainly activates the inner retinal neurons that are located more proximal than the photoreceptors.[5,6] Miyake et al.[7,8] have tried to use this technique for clinical diagnosis and evaluation of inner retinal function in patients with retinal diseases. Besides, TcES has become a potential tool to treat visual system disease in clinical practice because of the neuroprotective effects of electrical stimulation, such as improving retinal function in eyes with longstanding retinal artery occlusion,[9,10] protecting retinal neurons against ocular ischemia,[11] rescuing the axotomized retinal ganglion cells,[12] restoring the functional impairment of optic nerve injury,[13] and promoting photoreceptor survival after light injury.[14] With the development of retinal prostheses, the use of retinal-induced phosphenes evoked by TcES has been introduced to assess partially residual retinal function.[15–17] Moreover, Xie et al.[18] demonstrated that the retinotopic organization of primary visual cortex still is maintained in retina degeneration patients despite prolonged visual loss by using TcES. Therefore, TcES can be used to provide some indication of the retinocortical visual pathway function and preoperatively select suitable candidates for clinical trials. Although subjective measures have

a vital role in evaluation of residual visual function and candidate selection, objective measures also are essential. Measurement of neuronal activity in the central nervous system can objectively and quantitatively study the response properties to electrical stimulation, and thereby provide useful insights into neurophysiological mechanisms of visual prostheses.

Optical imaging of intrinsic signals (OIS) can monitor changes of brain activity at micron resolution and objectively reveal relatively large cortical areas. It has been used to estimate visual spatial resolution of cortical responses evoked by electrical stimulation of the retina.[19,20] Walter et al.[21] demonstrated that OIS could reveal the retinotopic activation of the visual cortex using a wireless-controlled retinal implant. Cloherty et al.[22] verified that localized activation of the cortex consistent with focal activation of the retina could be elicited by suprachoroidal electrical stimulation. Furthermore, Wong et al.[23] indicated that OIS was effective in imaging electrically evoked responses in the visual cortex, and could be used to improve implant designs and stimulation techniques for retinal prostheses. However, a more systematic study of the effect of electrical stimulation on the cortical responses based on OIS is needed.

The purpose of this study was to investigate the properties of cortical responses evoked by electrical stimulation of the retina. We used a multiwavelength OIS to record simultaneously the hemoglobin oxygenation changes and cerebral blood volume changes accompanying local neuronal activity. An ERG-jet corneal electrode placed on the stimulating eye was used to deliver different electrical stimuli with varied frequencies, pulse widths, and current intensities. Subdural evoked field potentials (EFPs) responding to TcES also were recorded for comparison from the imaging regions of visual cortex.

Methods

The methods of animal preparation and electrophysiological recording from visual cortex in cats have been described previously by Lu et al.[24] and are summarized briefly here.

Animal Preparation

We used 13 healthy adult cats (Fengxian, Shanghai, China) weighing between 2.0 and 3.0 kg in the experiments. All experimental procedures conformed to the guidelines of the Care and Use of Laboratory Animals issued by the National Institutes of Health (NIH) and the ARVO Statement for the Use of Animals in Ophthalmic and Vision Research, and were approved by the Ethics Committee of Shanghai Jiao Tong University. Initial anesthesia was induced with ketamine hydrochloride (20 mg/kg, intramuscularly), then atropine sulfate (0.15 mg/kg) and dexamethasone (25 mg/kg) were administrated intramuscularly to reduce salivation and cerebral edema. The cats were ventilated artificially by a pulmonary pump (Model 3000; Matrx, New York, NY, USA) and anesthetized with isoflurane (2%–3% during surgery, 1%–1.5% during recording). To maintain muscle relaxation and nutrition supply, a mixture of gallamine triethiodide (10 mg/kg/h) and glucose (24 mg/kg/h) was infused continuously intravenously. Temperature of the animal was kept at approximately 38°C by a water-circulating heating pad (T/Pump TP702; Gaymar Industries, New York, NY, USA). End-tidal carbon dioxide (CO_2), electrocardiogram (ECG), heart rate and pulse oximetry (SpO_2) were monitored continuously with a multiparameter life monitor (PM-8000 Express; Mindray, Shenzhen, China) throughout the experiments to ensure appropriate anesthetic depth. Eyes were covered with contact lenses of appropriate curvature such that the animal was focused on a screen. Before visual stimulation, the optic disks of cats were back-projected onto a screen. All the experiments were conducted in a dark room.

To record cortical responses, a craniotomy was performed at left hemisphere to expose visual areas 17 and 18 (Horsley–Clarke coordinates AP −8 to +8 mm, ML 0.5–6 mm). Dura of the cortex was removed after a 26-mm stainless steel chamber was cemented onto the cranium. The chamber was filled with warm silicone oil (DMPS-5X; Sigma-Aldrich Corp., St. Louis, MO, USA) and sealed with a round glass cover to reduce cortical vibration during recording. The imaging system was positioned on a floating vibration isolation platform to minimize motion artifacts.

Optical Imaging of Intrinsic Signals

Optical signals were acquired with a CCD camera (Dalsa 1M60, resolution 1024 × 1024 pixels; Dalsa Corporation, Waterloo, Canada), which is similar to those used by Pan et al.[25] The light from a halogen lamp was band-pass filtered (Lambda DG-4; Sutter Instruments, Novato, CA, USA) to provide illumination at three different wavelengths of 530 ± 10, 610 ± 10, and 630 ± 10 nm via a fiberoptic light guide. Illumination at isosbestic wavelength, such as 530 nm, allows imaging of changes in cerebral blood volume, whereas 600 to 630 nm allows imaging of changes in blood oxygenation.[26] The frame rate of the camera was 24 Hz, which was synchronized to filter switching, and, hence, an effective frame rate of 8 Hz was obtained for each wavelength. The image plane was focused at approximately 500 μ beneath the cortical surface. For each 24-second trial, recording started at 1 second before to the stimulus onset and lasted only 18 seconds, and consequently 144 frames of image were acquired simultaneously per wavelength.

Electrophysiological Recording

Multichannel subdural EFPs were captured by a neurophysiology workstation (RX7; Tucker-Davis Technologies, Alachua, FL, USA) at a 6-kHz sampling rate and band-pass filtered at 1 to 2000 Hz. A 4 × 10 silver-ball electrode array was fixed by a three-dimensional micromanipulator (MPA 2000; ALCBIO, Shanghai, China) and closely contacted the exposed visual cortex after the optical imaging. The interelectrode space is 1.6 mm (medial-lateral direction) × 1.2 mm (anterior-posterior direction), and the diameter of each silver-ball electrode is approximately 0.3 mm. The impedance of each electrode was measured by a Precision LCR Meter (E4980A; Agilent Technologies, Santa Clara, CA, USA) under 100 nA, 1 kHz sinusoidal current and ranged from 500 to 800 Ω. A screw electrode fixed to forehead skull was used as reference electrode and a stainless steel needle inserted into the ear tip as ground electrode.

Visual and Transcorneal Electrical Stimulation

Visual stimuli were generated by the user-defined MATLAB (MathWorks, Natick, MA, USA) program based on Psychtoolbox-3 and displayed on a gamma-corrected cathode ray tube (CRT) monitor (Dell P1130, 1280 × 960 pixels, 100 Hz; Dell, Round Rock, TX, USA) placed at 28.5 cm in front of the eyes. To obtain cortical orientation preference maps, the cats were stimulated binocularly with full-screen square-wave drifting gratings. The presented gratings involved 8 orientations (0°, 22.5°, 45°, 67.5°, 90°, 112.5°, 135°, 157.5°) and two spatial frequencies (0.58 and 0.14 cycles/deg [cpd]), which moved back and forth at a speed of 2 cycles/s (cps). The contrast of gratings was 100% with mean luminance of 30 cd/m^2. The

stimuli were presented continuously for 4 seconds, with an interstimulus interval (ISI) of 20 seconds using blank at mean luminance. Each block consisted of 8 different oriented gratings at the same spatial frequency followed by a blank trial appeared for 8 times. Totally, 16 to 20 blocks (one half for 0.58 cpd, the other half for 0.14 cpd) were completed in one experiment. The range of visual field elevation (from ~20° above to 4° below the horizontal meridian) was much wider than that of azimuth (~5° close to the vertical meridian) in our imaging regions.[27,28] Hence, we only used continuous-periodic stimuli horizontally oriented combined with a continuous acquisition paradigm to obtain the retinotopic elevation map.[29] The right eye of the cat was first stimulated with a horizontal bar (2° × 80°) drifting continuously in one direction for 48 cycles at a speed of 6°/s. Then, the stimulus bar drifted in the opposite direction for another 48 cycles.

A contact lens electrode (ERG-jet; CareFusion, Middleton, WI, USA) placed on the cornea surface of the right eye was used for TcES. Hydroxyethylcellulose gel (1.3%) was applied to protect the cornea, and keep good conductivity between the electrode and the cornea. A stainless steel needle inserted into the dorsal neck muscle ipsilateral to the stimulated eye was used as the return electrode. Biphasic charge-balanced rectangular cathode-first current pulses were generated by an isolated and programmable stimulating system (MS16; Tucker-Davis Technologies).

In optical imaging experiment, TcES was applied continuously for 2 seconds, with an ISI of 20 seconds in each trial. While changing electrical stimulation frequency, current intensity was set at 1.2 mA. To keep the total injected current charge constant, pulse width of the stimulation varied from 40 to 2 ms with stimulation frequency changing from 5 to 100 Hz. The following frequencies were used: 5, 10, 15, 20, 40, 60, 80, and 100 Hz, while the corresponding pulse widths per phase were: 40, 20, 13.3, 10, 5, 3.3, 2.5, and 2 ms. In the experiments studying effects of different stimulation pulse widths and current intensities, we kept stimulation frequency at 20 Hz, and used current intensities of 0.24, 0.36, 0.6, 0.84, 1.2, 1.68, 2.16, and 2.64 mA with 10 ms pulse width per phase, and pulse widths per phase of 2, 3, 5, 7, 10, 14, 18, and 22 ms with 1.2 mA intensity. Each block consisted of 8 different stimulus conditions followed by a blank trial repeated for 8 times. Totally, 16 to 20 blocks were finished for each experiment. In the electrophysiological experiment, shorter stimulation pulse width of 2 ms (frequency, 20 Hz; current intensity, 1.2 mA; stimulus duration, 2 seconds; ISI, 5 seconds) was used to reduce the artifact of electrical stimulation.

Data Analysis

All data analysis was performed using the user-defined MATLAB program. To minimize biological slow noise and correct uneven illumination, a map of light reflectance change (dR/R map) was obtained by subtracting and dividing blank image (binned from –1- to –0.25-second frames) then averaging trial-by-trial within one block.

For optical signals during visual stimulation, single-condition maps were calculated by averaging frames of dR/R map between 3 and 4 seconds after stimulus onset. Then, single-condition maps with orthogonal orientations were subtracted from each other to obtain differential orientation maps. All the differential orientation maps responding to gratings with the same spatial frequency were averaged across 8 to 10 blocks and then high-pass filtered (1.0–1.3 mm in diameter) and smoothed (170–272 μ in diameter) by circular averaging filters. Cells in area 17 were activated preferentially by gratings of high spatial frequency, whereas those in area 18 preferred stimulus with low spatial frequency.[30–32] To determine the border between areas 17 and 18, we averaged single-condition maps of 8 orientations at high spatial frequency 0.58 cpd then subtracted this image from that to gratings of low spatial frequency 0.14 cpd.[30] To generate contralateral retinotopic elevation map, a Fourier transformation was performed on the time course response of each pixel.[29] Then, we extracted the phase of the Fourier component at the frequency of stimulation and subtracted the reversed response phase from the direct response phase to obtain the map of absolute retinotopy. The elevation of visual field position for cortical location with maximum OIS response was estimated according to the retinotopic elevation map and stereotactic coordinates.[27,28]

The OIS at 600 to 630 nm is characterized predominantly as starting with an initial decrease, also termed initial dip, which is thought spatially to be most specific to local neuronal activity.[26,33] For optical signals during TcES, the dR/R maps were first collapsed into 250-ms frames to display the evolution of cortical responses. Single-condition maps were obtained by averaging over frames during initial dip (1.75–2.25 seconds after stimulus onset) and then over 16 to 20 blocks for a given stimulus condition. One 1.4 × 1.4 mm region of interest (ROI), with the greatest averaged reflectance decrement, was selected in single-condition map at 610 nm and used for subsequent analysis for all images at three wavelengths.[34] To avoid artifact due to large blood vessels, a vascular mask was created by thresholding the image illuminated with green light at 530 nm and pixels within this mask were excluded from further analysis.[35] We conducted 1-tailed *t*-test to evaluate cortical response to TcES and showed pixels with significantly ($P < 0.05$) decreased reflectance ratio in *P* value maps.[36] Signal-to-noise ratio (SNR) of optical responses at each wavelength was calculated as dividing peak amplitude by corresponding standard deviation of reflectance ratio in images 1 second before stimulus onset.

The optical responses to TcES in different frequencies were fitted with a Gaussian function $f(x) = a \cdot \exp(-(x - \mu)^2/2\sigma^2)$, where x is the stimulus frequency, $f(x)$ is the amplitude of response, a is the peak of the Gaussian curve, and σ is the width of the "bell curve," and μ is the position of the center of the peak and indicates the preferred frequency. The pulse width- and current intensity-dependent responses were respectively fitted using a Hill function $f(x) = v_{max} \cdot (x^n)/(x^n + k^n)$, where $f(x)$ is the amplitude of response, v_{max} is the maximum amount of response, x is the amount of pulse width or current intensity, k is the amount of pulse width or current intensity that reduces the amplitude of response by 50%, and n is the Hill coefficient.

For electrophysiological recording, trains of EFPs were averaged across 50 consecutive trials and filtered by a moving window of 1 ms. The EFP magnitude was determined as the amplitude difference between the first positive peak and the immediately followed negative peak.

For statistical analyses, Wilcoxon test was used for matched-pair data, and Mann–Whitney and Kruskal–Wallis tests were used for comparing independent data between two or more than two groups. $P < 0.05$ was considered statistically significant for all the tests.

Results

Spatiotemporal Patterns of Visual Cortical Responses Evoked by TcES

Figure 1A displays the evolution of optical responses to TcES as a sequence of 250-ms images. After stimulus onset, oximetric (610- and 630-nm response) signals had initial decreases shown

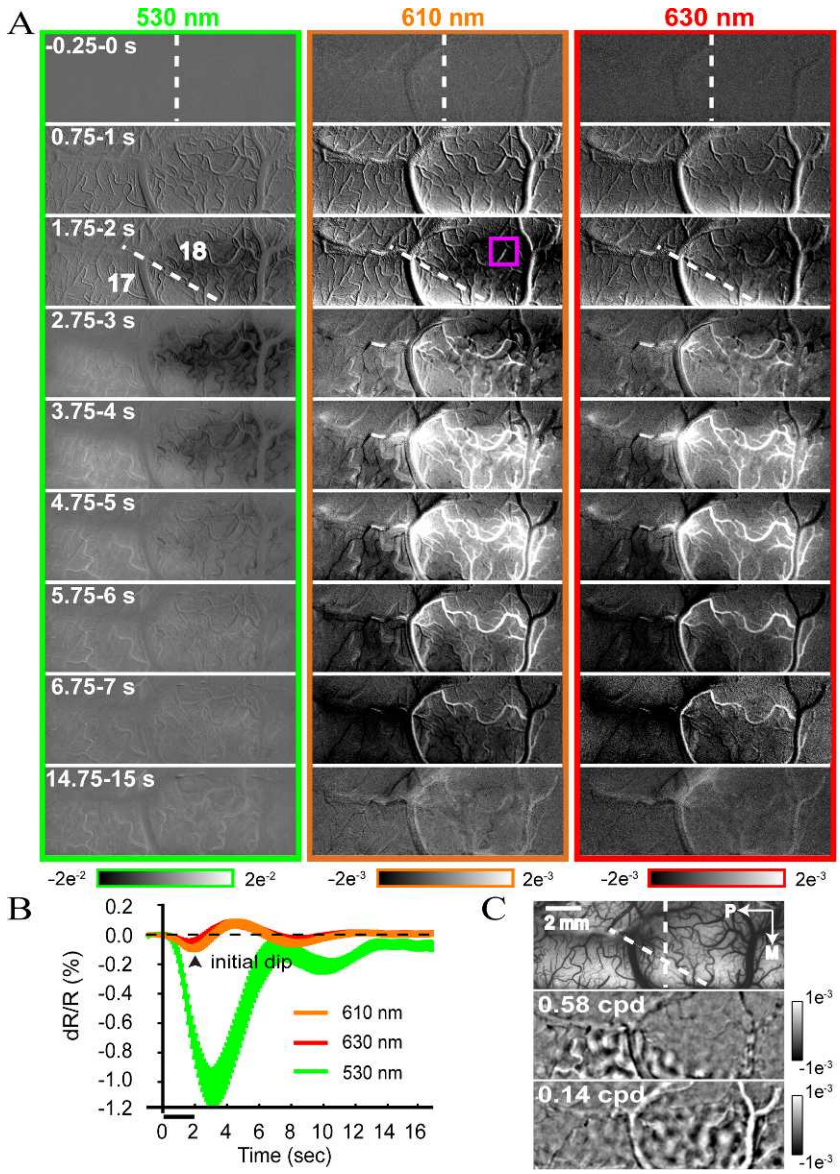

Figure 1. Spatiotemporal properties of cortical activation by TcES (stimulus duration, 2 seconds; frequency, 20 Hz; current intensity, 1.2 mA; pulse width, 10 ms). (**A**) High-resolution imaging of evoked cortical intrinsic signals under 530- (*green panel*), 610- (*orange panel*), and 630-nm (*red panel*) illumination, respectively. Data were averaged across 160 trials from one cat. Stimulus started at 0 seconds and lasted for 2 seconds. *Pink box* indicates ROI located at the activation regions for subsequent analysis. *Color bars* at the bottom represent reflectance change. (**B**) Temporal profiles of volumetric and oximetric signal changes averaged across 13 cats. *Black bar* denotes the stimulus duration (2 seconds). *Error bars* show the SEM. (**C**) The *top map* represents blood vessel map of cortical surface obtained at 530 nm. The *middle* and *bottom maps* represent differential orientation maps (0°–90°) to gratings with spatial frequency of 0.58 and 0.14 cpd. *Vertical* and *oblique lines* in (**A**, **C**) indicate the Horsley–Clarke coordinates AP0 and approximate area 17/18 border, respectively, which also shown in Figures 2 to 5 and 7. The area 17/18 border was obtained by subtracting the single-condition map elicited by a spatial frequency 0.58 cpd grating from the map by 0.14 cpd.[30] *Scale bar*: 2 mm. P, posterior; M, medial.

as pixels darkening in visual cortex, followed by a strong brightening, then a second darkening, and returned to baseline. In the volumetric (530-nm response) signal, a darkening area also appeared in visual cortex, and subsequently faded away. These spatial patterns of activation by TcES were observed in all 13 cats, which mainly located at area 18 according to the area 17/18 border (Fig. 1C).

To quantitatively compare properties of the volumetric and oximetric responses in 13 cats, temporal profiles of volumetric and oximetric responses within ROI (e.g., pink box in Fig. 1A) were shown in Figure 1B. Monophasic volumetric signal had a robust decrease peaked at 3.1 seconds (dR/R = −1.04 ± 0.12%) and gradually returned to baseline with some small fluctuations (Fig. 1B), whereas the oximetric signal at 610 nm was triphasic. It decreased after stimulus onset until 2.0 seconds (dR/R = −0.09 ± 0.01%) followed by a large rebound peaked at 4.6 seconds, then a delayed undershoot (secondary darkening, Fig. 1B). The peak response of volumetric signal was much higher than that of oximetric signal at 610 nm (−1.04% vs. −0.09%) and 630 nm (−1.04% vs. −0.04%) with identical response latencies. The SNR of the volumetric signal also was significantly larger than that of the oximetric signal (74.6 ± 10.5 vs. 20.3 ± 2.6 and 12.7 ± 1.8; Wilcoxon test, $P < 0.0005$, $n = 13$). The signal at 630 nm had a similar time course, but smaller magnitude. Moreover, the SNR of the 610-nm response was significantly higher than that of the 630-nm response (20.3

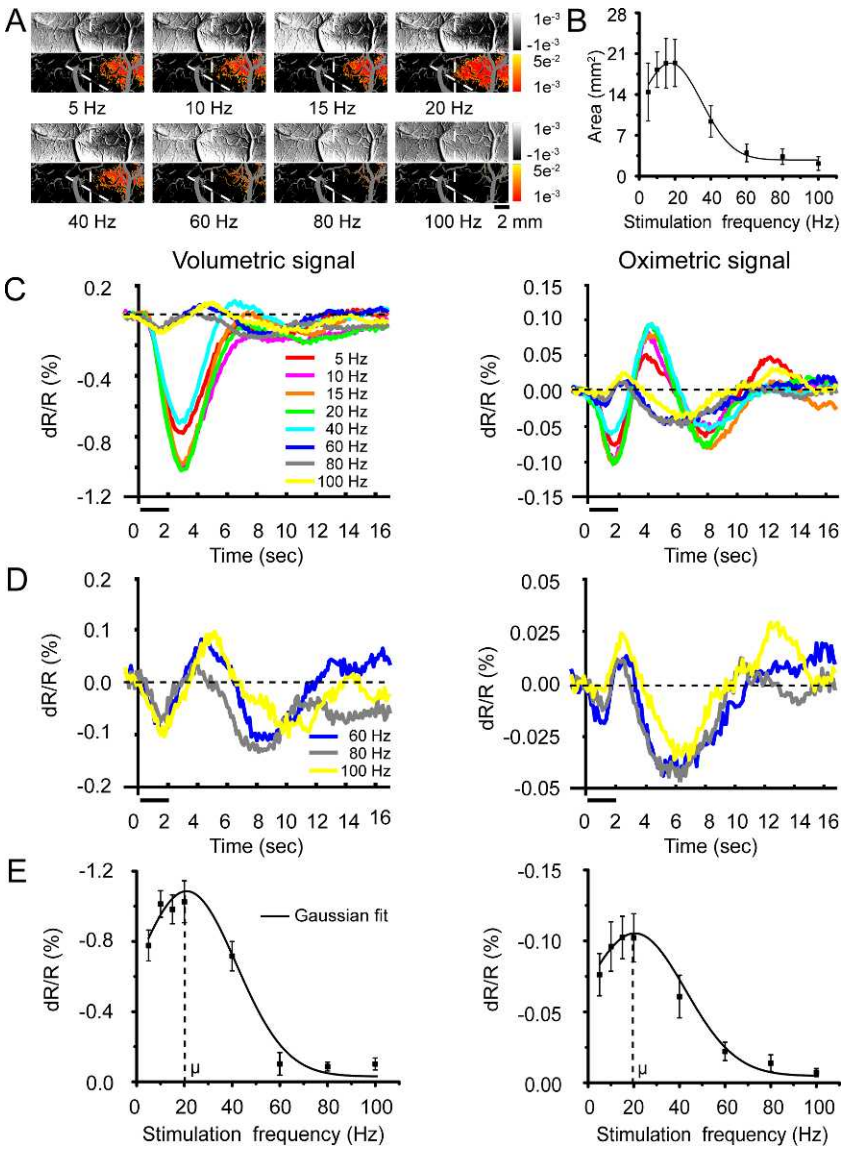

Figure 2. Effect of TcES frequency on cortical responses at constant electrical charge. (**A**) Optical single-condition maps and corresponding *P* value maps of 610-nm activation evoked by various stimulus frequencies. (**B**) Areas of statistically significant pixels ($P < 0.01$) in each *P* value map against stimulus frequencies ($n = 5$). (**C**) Time courses of volumetric and oximetric signals evoked by various stimulus frequencies. (**D**) Magnified view of time courses of volumetric and oximetric signals evoked by high-frequency (60, 80, and 100 Hz) stimuli. (**E**) Magnitudes of the initial optical signal decreases varied with different stimulus frequencies. Data were averaged over all of the pixels within selected ROI across five cats. *Error bars* indicate SEM.

± 2.6 vs. 12.7 ± 1.8; Wilcoxon test, $P < 0.005$, $n = 13$). Therefore, imaging illuminated at 630 nm was excluded from following analysis.

Effect of Changes in TcES Frequency

We investigated the effect of different TcES parameters on cortical responses. In single-condition maps to different TcES frequencies with current intensity of 1.2 mA, response regions were found mainly located in the anterior part of the craniotomy in area 18 (Fig. 2A). Spatial extent of activation areas as a *P* value map was displayed paired with a relevant single-condition map. Activated areas by low- (from 5–40 Hz) frequency stimuli obviously was larger than that by high- (from 60–100 Hz) frequency (Fig. 2B).

Time course of volumetric signal to TcES below 60 Hz in Figure 2C was almost the same, which had large declines (also shown in Fig. 1B). Similarly, all oximetric responses to stimuli from 5 to 40 Hz had pronounced initial dips. Volumetric and oximetric responses to high-frequency stimuli had much weaker and slightly earlier initial decreases (Fig. 2C; magnified view Fig. 2D). We used the valley values of initial decreases as indicators of response strength to TcES for different parameters, such as frequency, pulse width, and current intensity. The mean response amplitudes as a function of TcES frequencies are plotted and fitted with a Gaussian function in Figure 2E. The mean fitted preferred stimulus frequency (μ) from 5 cats was 19.9 ± 1.0 Hz (min, 17.0 Hz; max, 23.3 Hz) for the volumetric response and 19.5 ± 0.8 Hz (min, 17.2 Hz; max, 21.5 Hz) for the oximetric response. No significant differences were found between the mean response magnitude at 10, 15, and 20 Hz (Kruskal–Wallis test, oximetric, $P > 0.87$; volumetric, $P > 0.91$; $n = 5$).

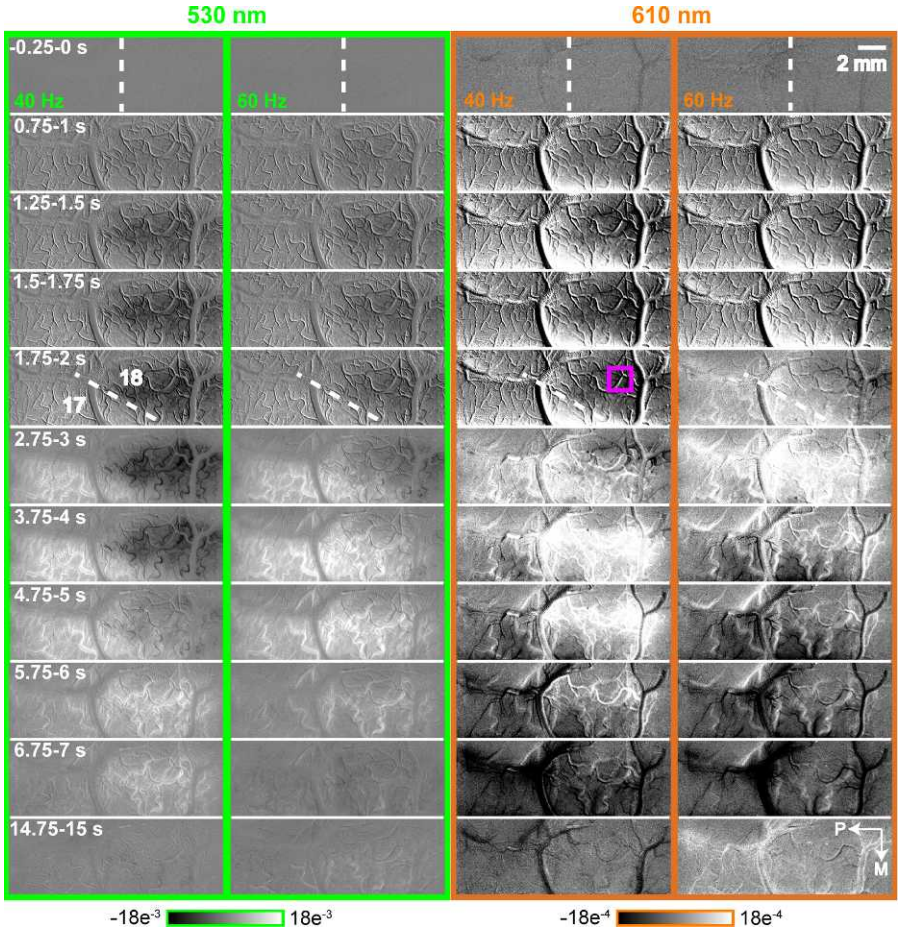

FIGURE 3. High-resolution imaging of cortical intrinsic signals evoked by low- (40 Hz) and high- (60 Hz) frequency stimuli, respectively. The *green panel* shows the evolution of optical responses evoked by low- (40 Hz) and high- (60 Hz) frequency stimuli under 530-nm illumination, respectively. The *orange panel* shows the evolution of optical responses evoked by low- (40 Hz) and high- (60 Hz) frequency stimuli under 610-nm illumination, respectively. Stimulus started at 0 seconds and lasted for 2 seconds. *Pink box* indicates ROI located at the activation regions. *Color bars* at the bottom represent reflectance change.

Since the differences between optical responses evoked by low- and high-frequency stimuli, we compared the spatiotemporal patterns of cortical responses to 40 and 60 Hz TcES (Fig. 3). To increase the detail, the time intervals of adjacent images were not always equal. As shown in the 530 nm panel, after 40 Hz TcES, a darkening area appeared, with the magnitude of response reached to the maximum at approximately 2.75 to 3 seconds, and subsequently slowly returned to baseline. However, the response to 60 Hz TcES achieved maximum at approximately 1.75 to 2 seconds. We can see clearly that the magnitude of response evoked by frequency of 60 Hz was much smaller than that evoked by frequency of 40 Hz. In the 610 nm panel, after 40 Hz TcES, a darkening area appeared (i.e., 610 nm initial dip), the dip had a rapid increase up to a maximum value at approximately 1.5 to 2 seconds, then followed by a strong brightening, and then a second darkening, and eventually returned to baseline, while the initial dip evoked by 60 Hz TcES reached to the maximum at approximately 1.25 to 1.75 seconds. The magnitude of response to 60 Hz TcES also was much smaller compared to that to 60 Hz TcES.

Effect of Changes in Stimulus Pulse Width

Effect of stimulus pulse widths ranging from 2 to 22 ms at 20 Hz and 1.2 mA on cortical OIS responses are shown in Figure 4. The significantly activated pixels mainly distributed in area 18; however, the activation area gradually extended to the 17/18 border while increasing pulse widths (Fig. 4A). The areas evoked by TcES dramatically enlarged with the pulse width increasing to 18 ms, then began to saturate (Fig. 4B).

The time courses of 530- and 610-nm responses (Fig. 4C) to short pulse width stimuli (2 and 3 ms) also showed weak response and phase advance as reported in response to high-frequency stimuli (Fig. 2C). In the volumetric and oximetric signals to different stimulus pulse widths, the mean reflectance changes to pulse width below 10 ms moved up sharply, then had a tendency to saturation. From Hill function–fitted curves, the pulse width to elicit half maximum response was estimated between 6.8 and 8.1 ms (Fig. 4D). Therefore, the effective TcES pulse width to evoke robust cortical OIS responses should be longer than 8 ms.

Effect of Changes in Stimulus Current Intensity

We measured the effect of various stimulus current intensities on cortical responses, with 20-Hz TcES frequency and 10-ms pulse width. The activating pixels in single-condition and *P* value maps were observed mainly in area 18, and more areas near the 17/18 border were activated while the current intensities increasing (Fig. 5A). The areas activated by TcES

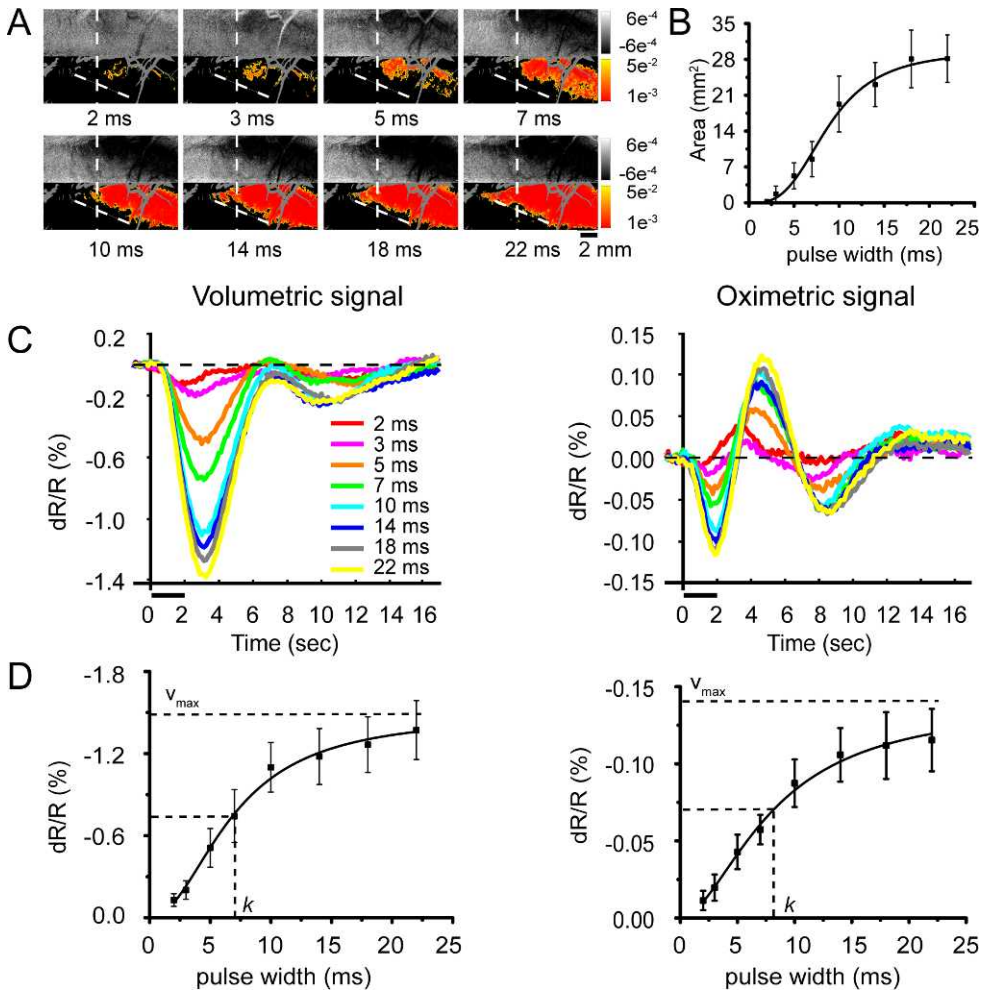

FIGURE 4. Effect of stimulus pulse width on cortical OIS responses. (**A**) Optical maps and corresponding *P* value maps of 610-nm activation evoked by various stimulus pulse widths. (**B**) Areas of statistically significant pixels ($P < 0.01$) in each *P* value map against stimulus pulse widths ($n = 7$). (**C**) Time courses of volumetric and oximetric signal changes evoked by stimuli of different pulse widths. (**D**) Magnitudes of the initial optical signal decreases varied with different stimulus pulse widths. Data were averaged over all of the pixels within selected ROIs across seven cats. *Error bars* indicate SEM.

expanded with the increment of current intensities, then saturated (Fig. 5B).

No phase advance was observed in the time courses of 530- and 610-nm responses in Figure 5C. From the Hill function–fitted curves, the current intensity evoking half-peak OIS response was estimated between 0.40 and 0.42 mA (Fig. 5D). Therefore, the threshold of current intensity for TcES was approximately 0.4 mA.

Effect of Stimulus Electric Charge

To compare the effect of electric charge/phase (i.e., the amplitude of pulse width × current intensity) on optical responses to 20 Hz TcES, electric charge-dependent response curves are shown in Figure 6. For each animal, the optical responses to different stimulus pulse widths and current intensities were normalized by the signal in response to electrical stimulation at 1.2-mA current intensity and 10-ms pulse width. Normalized amplitudes of volumetric and oximetric signals became stronger while increasing the electric charge of TcES. Under the same amount of charge injection, we compared the difference of effect on the normalized optical responses between increase in pulse width and increase in current intensity. We found that TcES below 12 μC/phase with longer pulse widths and smaller current intensities could elicit significant stronger responses (Mann–Whitney test, $P < 0.05$). Therefore, the effect of TcES pulse width on OIS responses were more prominent.

Electrophysiological Recording

We recorded subdural EFPs to investigate relationship between the OIS response pattern and neural activities at the same cortical areas evoked by TcES with the identical stimulus parameters. Figure 7 displays an example of comparison of optical and electrophysiological recording in response to TcES (stimulus duration, 2 seconds; frequency, 20 Hz; current intensity, 1.2 mA; pulse width, 2 ms). The curved contour line in Figure 7A indicates 65% of maximum reflectance change in the optical map. Figure 7B illustrates the recording of cortical positions of electrode array and optical imaging. The retinotopic elevation map shown in Figure 7C is similar to the result mapped electrophysiologically by Tusa et al.[27,28] The OIS response regions were located mainly in the anterior part of area 18, which represents the peripheral of lower visual field. The mean visual field elevation of the maximum OIS response from 3 cats was −16° ± 3° (min, −13°; max, −20°). Summed EFPs were considered as measurement of total neuronal

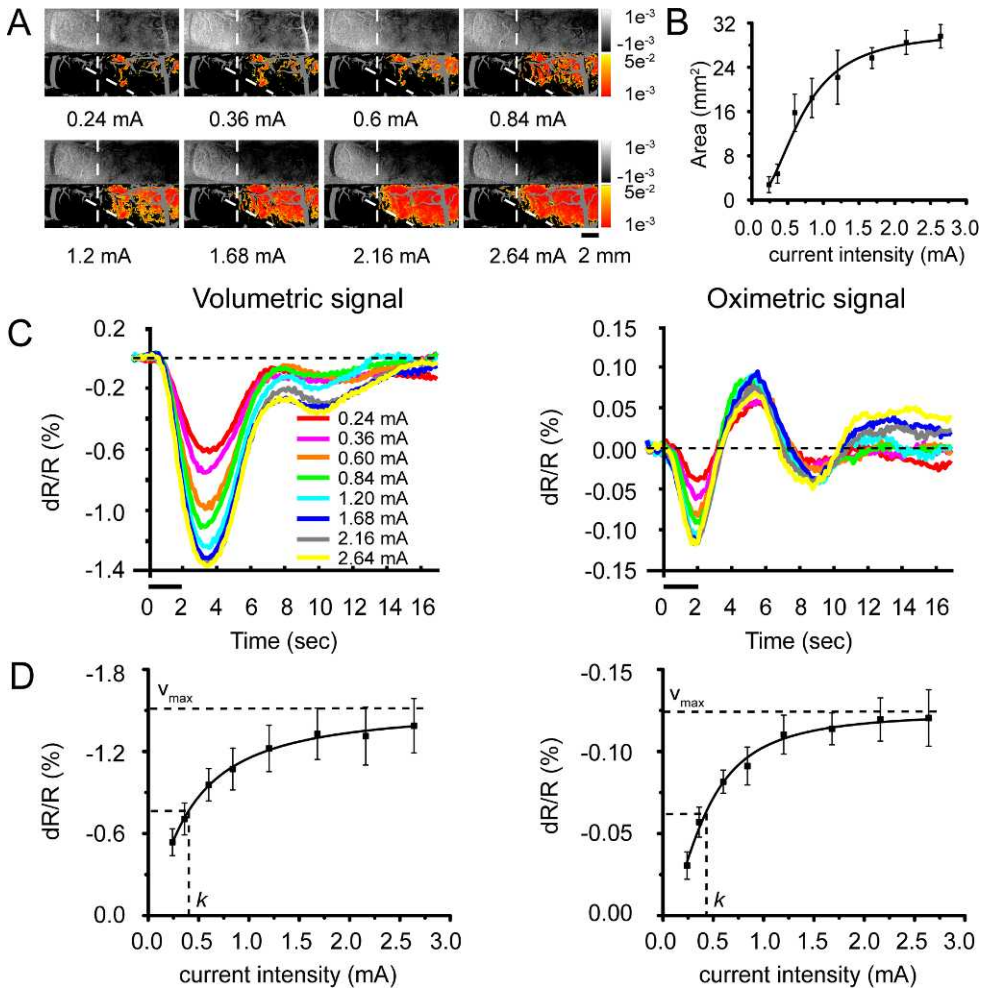

Figure 5. Effect of stimulus current intensity on cortical OIS responses. (**A**) Optical maps and corresponding *P* value maps of 610-nm activation evoked by various stimulus current intensities. (**B**) Areas of statistically significant pixels ($P < 0.01$) in each *P* value map against stimulus current intensities ($n = 6$). (**C**) Time courses of volumetric and oximetric signal changes evoked by stimuli of different current intensities. (**D**) Magnitudes of the initial optical signal decreases varied with different stimulus current intensities. Data were averaged over all of the pixels within selected ROIs across six cats. *Error bars* indicate SEM.

activity evoked by the stimulus.[34] Therefore, we calculated ΣEFP by averaging 40 amplitudes of all the EFPs within a 2-second stimulation trial (stimulation frequency, 20 Hz) for each channel. To directly compare the optical and electrophysiological signals in response to TcES, we then divided the optical map into 40 subregions corresponding to positions of 4×10 electrodes, and averaged the reflectance change over all of the pixels within each subregion. The scatter plot (Fig. 7E) showed

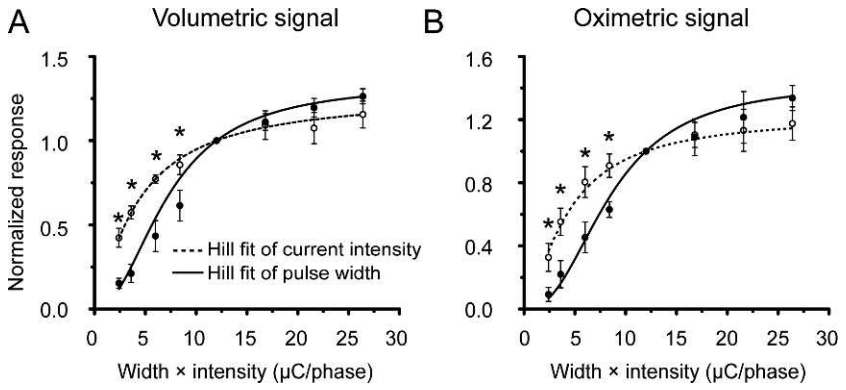

Figure 6. Comparison of OIS responses increased with different pulse widths and current intensities of TcES under same amount of electric charge at 20 Hz. (**A**) Comparison of volumetric responses. (**B**) Comparison of oximetric responses. Data were normalized to evoked optical signals by TcES at 1.2-mA current intensity, 10-ms pulse width, and averaged across animals ($n = 6$ for current intensity, $n = 7$ for pulse width). *Significantly different normalized response (Mann–Whitney test, $P < 0.05$). *Error bars* indicate SE.

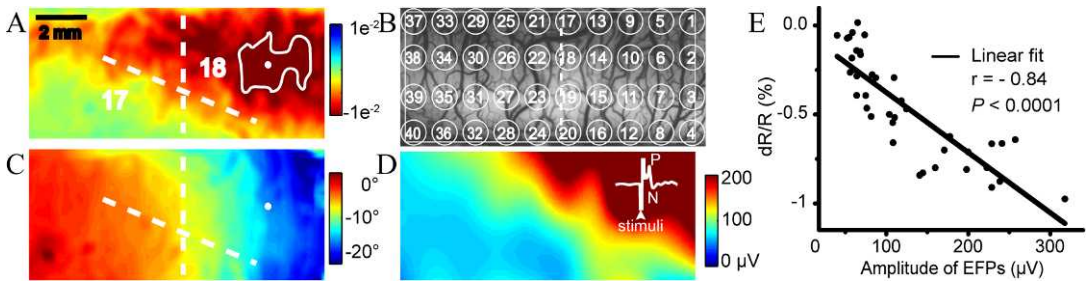

FIGURE 7. An example of comparison of optical and electrophysiological recording in response to TcES. (**A**) Optical map of activation evoked by TcES. The OIS response regions were defined as areas with reflectance change larger than 65% peak response, denoted by *curved line*. *White dot* (**A**, **C**) indicates the maximum OIS response. (**B**) Schematic illustration of the multichannel electrode array above the exposed cortical surface. *Circled number* represents each electrode of the array. *White rectangular box* indicates the optical imaging region. (**C**) The retinotopic elevation map smoothed by circular averaging filter (340 μ in diameter). (**D**) Spatial distribution color-coded map of ΣEFP amplitude smoothed by cubic interpolation. First waveform of EFP in the train responding to 20 Hz TcES by one electrode (number 10) located at the OIS response regions. Successive EFP waveforms in the trace are similar except for gradual attenuation in amplitude. P, positive peak; N, negative peak. *Arrowhead*: stimulus onset. (**E**) Correlation between the amplitudes of ΣEFP and the corresponding mean reflectance changes in OIS map.

a significant correlation ($r = -0.84$, $P < 0.0001$) between the amplitudes of ΣEFP and the corresponding mean reflectance changes in OIS map. The spatial distribution of ΣEFP is shown as a color-coded map of ΣEFP amplitudes recorded by 40 electrodes in Figure 7D. The EFP waveform recorded by an electrode within the response regions is shown as an inset. The regions with strong neuronal response were located primarily at cortical areas representing the peripheral visual field and they were well-matched with the response regions in the optical map.

DISCUSSION

The OIS has been used widely as a powerful tool for functionally characterizing naturally or electrically evoked response properties across sensory cortices.[37] Nonetheless, to our knowledge the optical responses in visual cortices evoked by TcES have never been investigated systematically. This study was done to investigate the spatiotemporal properties of cortical responses to TcES with OIS in cat experiments. The effects of different stimulus parameters on cortical responses were researched by manipulating stimulus frequency, pulse width, and current intensity. The EFPs in visual cortex also were recorded and the response regions detected by OIS exhibited strong neural responses.

We used the initial dip of 610-nm response, which was considered as the most specific measure of neuronal activity, to identify and localize the activation regions of the visual cortex. According to the stereotactic coordinates, our retinotopic map for elevation was similar to the retinotopic organization of visual cortex determined using electrophysiological mapping techniques by Tusa et al.[27,28] A small portion of area 17 in cats, which corresponds to roughly 5° around the central visual field, is exposed for our optical imaging. According to our results, the response regions of contralateral hemisphere evoked by TcES through ERG-jet contact lens electrodes were located mainly in the anterior part of the craniotomy in area 18. Activation of the anterior part of craniotomy in area 18, which represents the periphery of the lower right visual field, should correspond to the peripheral electrical stimulation of superior nasal retina as reported by Tusa et al.[27] The presence of OIS response in the anterior part of craniotomy in area 18 and absence of response in the exposed area 17 implied that ERG-jet stimulation largely acts on cells in the peripheral rather than central retina. The optical response was observed rarely in the posterior part of area 18 in our imaging region, which roughly represents the central 5° of the visual field. However, with the increment of current intensity or pulse width, we noticed that the response regions gradually extended to the intersection of the 17/18 border and AP0, which was close to the cortical representation of the area centralis. This indicated that more central retinal neurons were activated with the increment of TcES electric charge. Consistent with the optical imaging, much stronger EFPs response could be observed in the OIS response regions than the neighboring regions. We concluded that ERG-jet stimulation with return electrode on the ipsilateral dorsal neck muscle primarily activates the peripheral retina. This result was in agreement with a previous report that the peripheral retina is stimulated more strongly than the central retina by TcES.[38] Support for this view also can be found in a study on human in combination with positron emission tomography (PET) study and phosphene perception.[39] They demonstrated that ERG-jet stimulation preferentially activated the peripheral nasal retina by employing TcES modeling predictions.

We investigated different TcES parameters to elicit cortical responses efficiently and reliably. Many research groups have used 20 Hz as the stimulation frequency for research fields involved the TcES.[9,12,13,16,40] Retinal OIS signals elicited by transscleral electrical stimulation revealed that the maximal responses were obtained when the stimulus frequency was ranged from 15 to 20 Hz.[41] A major objective of this study was to quantitatively determine the frequency dependence of evoked cortical responses. The frequency distribution of cortical response was shown unimodal and the maximal responses were acquired with stimulus frequency from 10 to 20 Hz. These results also were in agreement with findings of a study in humans showing the maximum pupillary reflex and the brightest phosphene were elicited by TcES with a frequency of approximately 20 Hz.[42] In addition, blood flow increase at the optic nerve head induced by flicker stimulation,[43] visually evoked potentials,[44] and psychophysical studies using flickering stimuli[45] indicated maximal responses at approximately 20 Hz. In our studies, we found the phase advance accompanying extremely weak optical response evoked by high-frequency (60, 80, and 100 Hz) stimuli. The attenuation effect of higher stimulation frequency on hemodynamic response has been reported in the somatosensory cortex of the rat.[34,46] The differences between hemodynamic responses at high and low frequency make us believe that stimulus frequency is an important influence factor. However, the differences in actual sites within retina activated by different stimulation frequency still are unknown. Freeman et al.[47] measured the retinal cell response to sinusoidal electric stimulation of various frequencies in rabbits and their results

suggested that bipolar cells were activated preferentially at 25 Hz, while ganglion cells were activated at 100 Hz, which may contribute to these differences. Besides, in our experiments, the pulse width decreased from 40 to 2 ms with the frequency increasing from 5 to 100 Hz to keep the total injected charge constant. The effect of changes in pulse width of TcES on the retina (see below) also might influence the frequency-dependent response. As can be seen from Figure 4C, the phase advances accompanying extremely weak response at high frequency above 40 Hz appeared again in the shorter pulse width signals (especially at response to 2-ms electrical stimulation).

With 20-Hz frequency and 10-ms pulse width, Inomata et al.[41] reported that retinal responses elicited by transscleral electrical stimulation were strong above 0.4 mA in monkeys. Miyake et al.[48] found that the threshold current to evoke cortical potentials was 0.29 mA at 5-ms single pulse width in healthy individuals using a corneal contact electrode. Besides, Xie et al.[18] reported that the average threshold current of contact lens electrode to elicit phosphene was approximately 0.72 mA for five healthy individuals at 2 Hz with pulse width of 2 ms. These results were comparable to our threshold current of 0.4 mA at 10-ms pulse width and 20-Hz frequency. The variances may be due to differences in species, methods used for threshold determination, electrode type, and pulse width.

Our charge-response curves further showed that pulse width also is an important parameter. Under the same amount of charge injection (below 12 μC/phase), the longer pulse width stimulation can produce stronger response. In our work, to evoke intrinsic signals the efficient pulse width range was 10 to 15 ms (1.2 mA). We also found that more areas close to the 17/18 border can be evoked by longer pulse width stimulation, which suggested that the longer stimulus pulse width can activate the retinal cells at lower threshold of current intensity. In fact, several groups have demonstrated that the threshold to elicit phosphenes decreased with the increment of pulse width,[16,49] which was consistent with our finding. We interpreted this finding in the context of the different inner retinal mechanisms engaged respectively by shorter and longer pulse width stimulation.[50] The shorter pulse only evokes the action potentials in ganglion cells, whereas the longer pulse also acts on the retinal synaptic circuitry and can evoke sustained synaptic currents.

Preoperative evaluation of retinal and posterior visual pathway function is necessary before implantation of a retinal prosthesis. Noninvasive TcES already has been used as a screening tool to identify suitable recipients for the retinal prostheses. As TcES was used to evaluate visual function or to conduct a preoperative screening, the threshold of current intensity to generate phosphenes often is used as an assessment criterion. However, the threshold method in contact lens stimulation should be used carefully, because the threshold current in the central retina is much higher than the peripheral retina. A recent study in humans reported that the observed phosphenes sometimes were seen in the central visual field as current intensity increased.[16] Morimoto et al.[15] reported that phosphene elicited by TcES was first perceived in the peripheral field at low current intensity and it spread into the center of the visual field with the increase in current intensity. Another study showed that TcES with ERG-jet electrode in normal individuals resulted in a semilunate, crescent-shaped phosphene in the peripheral temporal visual field.[18] We presumed that this phenomenon was caused by the electrical stimulation with short pulse width and low current intensity, and therefore, probably activated the peripheral retina. Relative to the peripheral retinal function, the central retina function assessed by TcES is even more important for retinal prosthesis, which should be implanted in macular area. Appropriate selection of parameters for electrical stimulation will make the applications of retinal electrical stimulation more efficient. The results of this study provided an objective evaluation for the optimization of TcES parameters and would improve TcES performance on the assessment and screening in patients.

Normal sighted cats were used in our study instead of degenerated animal models. The ideal experimental design should use animal models with retinal degeneration, such as an animal model of RP. However, we believe that the efficient TcES parameters obtained in our study also are applicable in RP patients screening for retinal prosthesis implantation. First, the visual system of the cat is close to that of primates, so it is a suitable animal model for vision research. Second, the morphometric analyses in postmortem eyes have shown that approximately 80% of the inner retina neurons, which could be activated by TcES, in the macula[51] and 40% in the extramacular regions,[52] remain alive even in severe RP subjects. In addition, Xie et al.[18] demonstrated that the retinotopic organization of primary visual cortex still is maintained in patients with retinal degeneration despite prolonged visual loss. Hence, our results in normal sighted cats may provide some indication for the use of TcES in patients with retinal degenerative disease. However, since several studies showed the neural remodeling induced by retinal degenerations,[53,54] the efficient TcES parameters in our study should be adjusted carefully when directly translated into the clinical conditions.

In conclusion, spatiotemporal patterns of visual cortical responses during TcES were reported in this study. The response regions evoked by TcES through ERG-jet contact lens electrode were located mainly in cortical areas representing peripheral visual field. We demonstrated that the OIS response regions were accompanied by strong evoked field potentials. With the increase of TcES current intensity or pulse width, we noticed that the response regions extended gradually from the cortical areas representing peripheral visual field to the areas representing central visual field. The largest optical responses were acquired with the stimulus frequencies between 10 and 20 Hz. These results contributed to the comprehension of the neurophysiological underpinnings of prosthetic vision and also facilitated the application of retinal electrical stimulation using TcES.

Acknowledgments

The authors thank Wei Wang (at Institute of Neuroscience, CAS) for useful comments on the manuscript.

Supported by The National Basic Research Program of China (973 Program, 2011CB707503/2), The National Natural Science Foundation of China (61273368, 91120304, 61171174), National High Technology Research and Development Program of China (863 Program, 2009AA04Z326), Shanghai Municipal Physical Culture Bureau Scientific and Technological Project (11JT010), and The 111 Project from the Ministry of Education of China (B08020).

Disclosure: **Z. Ma**, None; **P. Cao**, None; **P. Sun**, None; **L. Li**, None; **Y. Lu**, None; **Y. Yan**, None; **Y. Chen**, None; **X. Chai**, None

References

1. Shepherd RK, Shivdasani MN, Nayagam DA, Williams CE, Blamey PJ. Visual prostheses for the blind. *Trends Biotechnol*. 2013;31:562–571.
2. Stronks HC, Barry MP, Dagnelie G. Electrically elicited visual evoked potentials in Argus II retinal implant wearers. *Invest Ophthalmol Vis Sci*. 2013;54:3891–3901.
3. Merabet LB, Rizzo JF, Pascual-Leone A, Fernandez E. 'Who is the ideal candidate?': decisions and issues relating to visual

neuroprosthesis development, patient testing and neuroplasticity. *J Neural Eng*. 2007;4:S130–S135.

4. Potts AM, Inoue J, Buffum D. The electrically evoked response of the visual system (EER). *Invest Ophthalmol*. 1968;7:269–278.
5. Potts AM, Inoue J. The electrically evoked response of the visual system (EER). 3. Further contribution to the origin of the EER. *Invest Ophthalmol*. 1970;9:814–819.
6. Shimazu K, Miyake Y, Watanabe S. Retinal ganglion cell response properties in the transcorneal electrically evoked response of the visual system. *Vision Res*. 1999;39:2251–2260.
7. Miyake Y, Yanagida K, Yagasaki K. [Clinical application of EER (electrically evoked response). Analysis of EER in patients with optic nerve disease (author'seconds transl)]. *Nippon Ganka Gakkai Zasshi*. 1980;84:2047–2052.
8. Miyake Y, Hirose T, Hara A. Electrophysiologic testing of visual functions for vitrectomy candidates. I. Results in eyes with known fundus diseases. *Retina*. 1983;3:86–94.
9. Inomata K, Shinoda K, Ohde H, et al. Transcorneal electrical stimulation of retina to treat longstanding retinal artery occlusion. *Graefes Arch Clin Exp Ophthalmol*. 2007;245:1773–1780.
10. Oono S, Kurimoto T, Kashimoto R, Tagami Y, Okamoto N, Mimura O. Transcorneal electrical stimulation improves visual function in eyes with branch retinal artery occlusion. *Clin Ophthalmol*. 2011;5:397–402.
11. Wang X, Mo X, Li D, et al. Neuroprotective effect of transcorneal electrical stimulation on ischemic damage in the rat retina. *Exp Eye Res*. 2011;93:753–760.
12. Morimoto T, Miyoshi T, Matsuda S, Tano Y, Fujikado T, Fukuda Y. Transcorneal electrical stimulation rescues axotomized retinal ganglion cells by activating endogenous retinal IGF-1 system. *Invest Ophthalmol Vis Sci*. 2005;46:2147–2155.
13. Miyake K, Yoshida M, Inoue Y, Hata Y. Neuroprotective effect of transcorneal electrical stimulation on the acute phase of optic nerve injury. *Invest Ophthalmol Vis Sci*. 2007;48:2356–2361.
14. Ni YQ, Gan DK, Xu HD, Xu GZ, Da CD. Neuroprotective effect of transcorneal electrical stimulation on light-induced photoreceptor degeneration. *Exp Neurol*. 2009;219:439–452.
15. Morimoto T, Fukui T, Matsushita K, et al. Evaluation of residual retinal function by pupillary constrictions and phosphenes using transcorneal electrical stimulation in patients with retinal degeneration. *Graefes Arch Clin Exp Ophthalmol*. 2006;244:1283–1292.
16. Huang Q, Chowdhury V, Coroneo MT. Evaluation of patient suitability for a retinal prosthesis using structural and functional tests of inner retinal integrity. *J Neural Eng*. 2009;6:035010.
17. Yanai D, Lakhanpal RR, Weiland JD, et al. The value of preoperative tests in the selection of blind patients for a permanent microelectronic implant. *Trans Am Ophthalmol Soc*. 2003;101:223–228, discussion 228–230.
18. Xie J, Wang GJ, Yow L, et al. Preservation of retinotopic map in retinal degeneration. *Exp Eye Res*. 2012;98:88–96.
19. Eckhorn R, Wilms M, Schanze T, et al. Visual resolution with retinal implants estimated from recordings in cat visual cortex. *Vision Res*. 2006;46:2675–2690.
20. Eysel UT, Walter P, Gekeler F, et al. Optical imaging reveals 2-dimensional patterns of cortical activation after local retinal stimulation with sub- and epiretinal visual prostheses. *Invest Ophthalmol Vis Sci*. 2002;43:1284–1284.
21. Walter P, Kisvarday ZF, Gortz M, et al. Cortical activation via an implanted wireless retinal prosthesis. *Invest Ophthalmol Vis Sci*. 2005;46:1780–1785.
22. Cloherty SL, Hietanen MA, Suaning GJ, Ibbotson MR. Focal activation of primary visual cortex following supra-choroidal electrical stimulation of the retina: Intrinsic signal imaging and linear model analysis. *32th Annu Int Conf IEEE Eng Med Bio Soc*. 2010;6765–6768.
23. Wong YT, Hallum LE, Chen SC, et al. Optical imaging of electrically evoked visual signals in cats: I. Responses to corneal and intravitreal electrical stimulation. *29th Annu Int Conf IEEE Eng Med Bio Soc*. 2007;1635–1638.
24. Lu Y, Yan Y, Chai X, Ren Q, Chen Y, Li L. Electrical stimulation with a penetrating optic nerve electrode array elicits visuotopic cortical responses in cats. *J Neural Eng*. 2013;10:036022.
25. Pan YX, Chen MG, Yin JP, et al. Equivalent representation of real and illusory contours in Macaque V4. *J Neurosci*. 2012;32:6760–6770.
26. Frostig RD, Lieke EE, Ts'o DY, Grinvald A. Cortical functional architecture and local coupling between neuronal activity and the microcirculation revealed by in vivo high-resolution optical imaging of intrinsic signals. *Proc Natl Acad Sci U S A*. 1990;87:6082–6086.
27. Tusa RJ, Rosenquist AC, Palmer LA. Retinotopic organization of areas 18 and 19 in the cat. *J Comp Neurol*. 1979;185:657–678.
28. Tusa RJ, Palmer LA, Rosenquist AC. The retinotopic organization of area 17 (striate cortex) in the cat. *J Comp Neurol*. 1978;177:213–235.
29. Kalatsky VA, Stryker MP. New paradigm for optical imaging: temporally encoded maps of intrinsic signal. *Neuron*. 2003;38:529–545.
30. Huang LX, Chen X, Shou TD. Spatial frequency-dependent feedback of visual cortical area 21a modulating functional orientation column maps in areas 17 and 18 of the cat. *Brain Res*. 2004;998:194–201.
31. Hung CP, Ramsden BM, Chen LM, Roe AW. Building surfaces from borders in Areas 17 and 18 of the cat. *Vision Res*. 2001;41:1389–1407.
32. Issa NP, Trepel C, Stryker MP. Spatial frequency maps in cat visual cortex. *J Neurosci*. 2000;20:8504–8514.
33. Malonek D, Dirnagl U, Lindauer U, Yamada K, Kanno I, Grinvald A. Vascular imprints of neuronal activity: relationships between the dynamics of cortical blood flow, oxygenation, and volume changes following sensory stimulation. *Proc Natl Acad Sci U S A*. 1997;94:14826–14831.
34. Sheth S, Nemoto M, Guiou M, Walker M, Pouratian N, Toga AW. Evaluation of coupling between optical intrinsic signals and neuronal activity in rat somatosensory cortex. *Neuroimage*. 2003;19:884–894.
35. Sirotin YB, Hillman EMC, Bordier C, Das A. Spatiotemporal precision and hemodynamic mechanism of optical point spreads in alert primates. *Proc Natl Acad Sci U S A*. 2009;106:18390–18395.
36. Tanigawa H, Lu HD, Roe AW. Functional organization for color and orientation in macaque V4. *Nat Neurosci*. 2010;13:1542–1548.
37. Zepeda A, Arias C, Sengpiel F. Optical imaging of intrinsic signals: recent developments in the methodology and its applications. *J Neurosci Methods*. 2004;136:1–21.
38. Kawasumi M. [Distribution of current intensities inside the electrically stimulated eye]. *Nippon Ganka Gakkai Zasshi*. 1985;89:766–772.
39. Xie J, Wang GJ, Yow L, et al. Modeling and percept of transcorneal electrical stimulation in humans. *IEEE Trans Biomed Eng*. 2011;58:1932–1939.
40. Schatz A, Rock T, Naycheva L, et al. Transcorneal electrical stimulation for patients with retinitis pigmentosa: a prospective, randomized, sham-controlled exploratory study. *Invest Ophthalmol Vis Sci*. 2011;52:4485–4496.
41. Inomata K, Tsunoda K, Hanazono G, et al. Distribution of retinal responses evoked by transscleral electrical stimulation

Investigative Ophthalmology & Visual Science

detected by intrinsic signal imaging in macaque monkeys. *Invest Ophthalmol Vis Sci*. 2008;49:2193–2200.

42. Fujikado T, Morimoto T, Kanda H, et al. Evaluation of phosphenes elicited by extraocular stimulation in normals and by suprachoroidal-transretinal stimulation in patients with retinitis pigmentosa. *Graefes Arch Clin Exp Ophthalmol*. 2007;245:1411–1419.
43. Van Toi V, Riva C. Variations of blood flow at optic nerve head induced by sinusoidal flicker stimulation in cats. *J Physiol*. 1995;482:189–202.
44. Regan D. A high frequency mechanism which underlies visual evoked potentials. *Electroenceph Clin Neurophysiol*. 1968;25:231–237.
45. Kelly DH. Visual response to time-dependent stimuli. I. Amplitude sensitivity measurements. *J Opt Soc Am*. 1961;51:422–429.
46. Martin C, Martindale J, Berwick J, Mayhew J. Investigating neural-hemodynamic coupling and the hemodynamic response function in the awake rat. *Neuroimage*. 2006;32:33–48.
47. Freeman DK, Eddington DK, Rizzo JF, Fried SI. Selective activation of neuronal targets with sinusoidal electric stimulation. *J Neurophysiol*. 2010;104:2778–2791.
48. Miyake Y, Yanagida K, Yagasaki K. [Clinical application of EER (electrically evoked response). (1) Analysis of EER in normal subjects (author's transl)]. *Nippon Ganka Gakkai Zasshi*. 1980;84:354–360.
49. Gekeler F, Messias A, Ottinger M, Bartz-Schmidt KU, Zrenner E. Phosphenes electrically evoked with DTL electrodes: a study in patients with retinitis pigmentosa, glaucoma, and homonymous visual field loss and normal subjects. *Invest Ophthalmol Vis Sci*. 2006;47:4966–4974.
50. Margalit E, Thoreson WB. Inner retinal mechanisms engaged by retinal electrical stimulation. *Invest Ophthalmol Vis Sci*. 2006;47:2606–2612.
51. Santos A, Humayun MS, deJuan E, et al. Preservation of the inner retina in retinitis pigmentosa–a morphometric analysis. *Arch Ophthalmol*. 1997;115:511–515.
52. Humayun MS, Prince M, de Juan E Jr, et al. Morphometric analysis of the extramacular retina from postmortem eyes with retinitis pigmentosa. *Invest Ophthalmol Vis Sci*. 1999;40:143–148.
53. Marc RE, Jones BW, Watt CB, Strettoi E. Neural remodeling in retinal degeneration. *Prog Retin Eye Res*. 2003;22:607–655.
54. Marc RE, Jones BW. Retinal remodeling in inherited photoreceptor degenerations. *Mol Neurobiol*. 2003;28:139–147.

Investigative Ophthalmology & Visual Science